Trends in

Applied Sciences Research

ISSN 1819-3579

Academic
Journals Inc.

www.academicjournals.com

Trends in Applied Sciences Research 7 (5): 370-381, 2012
ISSN 1819-3579 / DOI: 10.3923/tasr.2012.370.381
© 2012 Academic Journals Inc.

Carrier Density and Photon Rates Distributions of the Active Region of a Wideband Semiconductor Optical Amplifiers

O. Mahran, M.T. Al Absy, M.S. Helmy and G.D. Roston
Department of Physics, Faculty of Science, Alexandria University, Alexandria, Egypt

Corresponding Author: O. Mahran, Department of Physics,Faculty of Science, Alexandria University, Alexandria, Egypt

ABSTRACT

Spatial distributions of the carrier density and photon rates along the active region of a bulk InP-InGaAsP semiconductor optical amplifier are investigated under the effect of the change a set of parameters such as input signal power, bias current, arsenide molar fraction and temperature. It is found that the average free carrier density decreases with increasing the input power. At low input power, the carrier density has a symmetrical spatial distribution, while at high input powers; the carrier density spatial distribution becomes more asymmetrical. The effect of increasing the bias current is to increase the Semiconductor Optical Amplifiers (SOA) carrier density and the signal and total Amplified Spontaneous Emission (ASE) photon rates. Although the carrier density increases with increasing the temperature, the signal and total ASE photon rates decrease with temperature, so analysis of these spatial distributions can be used to aid SOA design.

Key words: SOA, carrier density, photon rates, traveling-wave equations

INTRODUCTION

The use of Semiconductor Optical Amplifiers (SOA) is currently of considerable interest for applications in long-haul optical fiber communication systems. SOAs are used mainly in the 1.5 μm wavelength region and as such are fabricated from the same materials used to fabricate laser sources in these regions (Agrawal, 2002). Earlier studies proposed that time dependent rate equations are inadequate for a SOA whose end faces have been covered with antireflection coatings (Marcuse, 1983).

Therefore, in order to present a clearer picture of the amplification process within the SOA, spatial dependence of the carrier density and signal field and spontaneous emission photon rates must be taken into account. Analysis of these spatial distributions can be used to aid SOA design. For this reason, the photon distribution in the SOA is described by means of time and space dependent traveling-wave equations. The incoherent spontaneous emission noise is described by traveling-wave power equations while the signal is described by a coherent traveling-wave amplitude equation.

In this study, we consider the active region of the SOA fabricated from bulk InP-In_{1-x} Ga_x As_y P_{1-y} direct bandgap material. y and x are molar fractions of Arsenide and Gallium, respectively, in the undoped active region, the SOA carrier density spatial variation, forward and backward-propagating signal photon rates and the total Amplified Spontaneous Emission (ASE)

photon rates distributions are studied under the effect of the change a set of parameters such as input signal power, bias current, arsenide molar fraction and temperature.

THEORETICAL MODEL

Based on the wideband model for SOA proposed (Connelly, 2001), the InGaAsP direct bandgap bulk material active region has a material gain coefficient g_m given by:

$$g_m(\nu,n) = \frac{c^2}{4\sqrt{2}\pi^{3/2} n_r^2 \nu^2 \tau_{rad}} \left(\frac{2m_e m_{hh}}{\hbar(m_e + m_{hh})} \right)^{3/2} \sqrt{\nu - \frac{E_g(n)}{h}} \left(f_c(\nu) - f_v(\nu)\right) \tag{1}$$

Where:

c	:	Speed of light in a vacuum
v	:	Optical frequency
n_1	:	Active region refractive index
τ_{rad}	:	Radiative carrier recombination lifetime
h	:	Planck's constant h divided by 2π
m_e,m_{hh}	:	Conduction Band (CB) electron and Valence Band (VB) heavy hole effective masses, respectively
n CB	:	Carrier (electron) concentration
f_c(v)	:	Occupation probability of an electron with frequency v in the CB
f_v(v)	:	Occupation probability of an electron with frequency v in the VB

The bandgap energy E_g can be expressed as (Connelly, 2001):

$$E_g(n) = E_{g0} - \Delta E_g(n) \tag{2}$$

where, E_{g0} is the bandgap energy with no injected carriers and is given by the quadratic approximation (Gillner, 1992):

$$E_{g0} = e(a + by + cy^2) \tag{3}$$

where, a, b and c are the quadratic coefficients and e is the electronic charge. ΔE_g(n) is the bandgap shrinkage due to the injected carrier density given by Lowery (1990):

$$\Delta E_g(n) = eK_g n^{1/3} \tag{4}$$

where, K_g is the bandgap shrinkage coefficient.

The total loss coefficient, α(n), of an SOA active region can be modeled by Connelly (2001):

$$\alpha(n) = K_0 + \Gamma K_1 n \tag{5}$$

where, K_0 and K_1 are carrier independent and carrier dependent absorption loss coefficients, respectively. K_0 represents the intrinsic material loss and K_1 is mainly due to intervalence band absorption.

In the amplifier, the spatially varying component of the field due to the input signal can be decomposed into two complex traveling-waves: E^+_s and E^-_s propagating in the positive and negative z directions respectively which obey the following complex differential equations (Connelly, 2001):

$$\frac{dE_s^+(z)}{dz} = \left(-j\beta + \frac{1}{2}\left[\Gamma g_m(\nu, n) - \alpha(n)\right]\right)E_s^+ \tag{6}$$

$$\frac{dE_s^-(z)}{dz} = \left(j\beta - \frac{1}{2}\left[\Gamma g_m(\nu, n) - \alpha(n)\right]\right)E_s^- \tag{7}$$

where, $j=\sqrt{-1}$ and $\boldsymbol{\beta}$ is the signal propagation coefficient which is given by Adachi (1992):

$$\beta = \frac{2\pi n_{eq}\nu}{c} \tag{8}$$

where n_{eq} is the equivalent index of the amplifier.

It is assumed that the modulus squared of the amplitude of the traveling-wave is equal to the photon rate of the wave in that direction, so:

$$N_s^+ = \left|E_s^+\right|^2 \text{ and } N_s^- = \left|E_s^-\right|^2 \tag{9}$$

The amplification of the signal also depends on the amount of spontaneously emitted noise generated by the amplifier. This is because the noise power takes part in draining the available carrier population. It is sufficient to describe the spontaneous emission in terms of power, while signals must be treated in terms of waves with definite amplitude and phase.

The spontaneous emission photon rates N^+_j and N^-_j (s^{-1}) in the positive and negative directions along the amplifier axis respectively obey the traveling-wave equations (Connelly, 2001):

$$\frac{dN_j^+(z)}{dz} = \left(\Gamma g_m(\nu_j, n) - \alpha(n)\right)N_j^+ + R_{sp}(\nu_j, n) \tag{10}$$

and:

$$\frac{dN_j^-(z)}{dz} = -\left(\Gamma g_m(\nu_j, n) - \alpha(n)\right)N_j^- + R_{sp}(\nu_j, n) \tag{11}$$

The function $R_{sp}(v_j, n)$ represents the spontaneously emitted noise coupled into N^+_j or N^-_j.

The amplifier material gain and spontaneous emission originate from carriers injected into the active region by the bias current. The carrier density (m^{-3}) at position z in the amplifier obeys the rate equation (Nilsson, 1978):

$$\begin{aligned}\frac{dn(z)}{dt} = \frac{I}{edLW} - R(n(z)) - \frac{\Gamma}{dW}\left\{\sum_{k=1}^{N_s} g_m(\nu_k, n(z))\left[N_{s_k}^{+}(z) + N_{s_k}^{-}(z)\right]\right\} \\ - \frac{2\Gamma}{dW}\left\{\sum_{j=0}^{N_m-1} g_m(\nu_j, n(z))K_j\left[N_j^{+}(z) + N_j^{-}(z)\right]\right\}\end{aligned} \quad (12)$$

where, I is the amplifier bias current, d and W are the active region thickness and width, respectively.

The first term on the RHS of Eq. 12 represents the addition of carriers to the active region from the bias current. These injected carriers are then depleted by various mechanisms occurring within the amplifier. The second term is due to radiative and nonradiative recombination mechanisms. The third and fourth terms represent radiative recombination of carriers due to the amplified signal and ASE. Γ is included as only this fraction of amplified photons resides in the active region. The factor of two in Eq. 12 accounts for the fact that spontaneously emitted photons can exist in one of two mutually orthogonal polarizations (TE or TM).

The recombination rate term R(n) is given by Wolff (1962):

$$R(n) = R_{rad}(n) + R_{nrad}(n) \quad (13)$$

where, $R_{rad}(n)$ and $R_{nrad}(n)$ are the radiative and nonradiative carrier recombination rates, respectively. Both of which can be expressed as polynomial functions of n (Olshansky *et al.*, 1984; Kot and Zdansky, 1992):

$$R_{rad}(n) = A_{rad}n + B_{rad}n^2 \quad (14)$$

$$R_{nrad}(n) = A_{nrad}n + B_{nrad}n^2 + C_{aug}n^3 + D_{leak}n^{5.5} \quad (15)$$

In Eq. 14, A_{rad} and B_{rad} are the linear and bimolecular radiative recombination coefficients. In Eq. 15, A_{nrad} is a linear nonradiative recombination coefficient due to traps in the semiconductor material (Kot and Zdansky, 1992). B_{nrad} represents nonradiative bimolecular recombination. C_{aug} is the Auger recombination coefficient and D_{leak} represents recombination due to leakage effects. As the SOA model equations cannot be solved analytically, a numerical solution is required. SOA geometrical and material parameters used in the steady-state model are given in Table 1 (Connelly, 2001).

RESULTS AND DISCUSSION

Input power effect: Figure 1 shows the simulated free carrier density distribution versus the position along the active region for three different injected signal powers, -40, -20 and -10 dBm. The forward and backward signal photon rates at -40 and -10 dBm input powers are shown in Fig. 2 and 3, respectively.

Table 1: SOA geometrical and material parameters used in the steady-state model (Connelly, 2001)

Symbol	Parameter	Value
y	Molar fraction of Arsenide in the active region	0.892
L	Active region length	700 μm
d	Active region thickness	0.4 μm
W	Active region width	0.4 μm
Γ	Optical confinement factor	0.45
K_g	Bandgap shrinkage coefficient	0.9×0^{-10} eVm
n_1	InGaAsP active region refractive index	3.22
n_2	InP region refractive index	3.167
η_{in}	Input coupling loss	3.0 dB
η_{out}	Output coupling loss	3.0 dB
R_1	Input facet reflectivity	5.0×0^{-5}
R_2	Output facet reflectivity	5.0×0^{-5}
K_0	Carrier independent absorption loss coefficient	6200 m^{-1}
K_1	Carrier dependent absorption loss coefficient	7500×0^{-24} m^2
A_{rad}	Linear radiative recombination coefficient	1.0×0^{7} s^{-1}
B_{rad}	Bimolecular radiative recombination coefficient	5.6×0^{-16} m^3 s^{-1}
A_{nrad}	Linear nonradiative recombination coefficient due to traps	3.5×0^{8} s^{-1}
B_{nrad}	Bimolecular nonradiative recombination coefficient	0.0×0^{-16} m^3 s^{-1}
C_{aug}	Auger recombination coefficient	3.0×0^{-41} m^6 s^{-1}
D_{leak}	Leakage recombination coefficient	0.0×0^{48} $m^{13.5}$ s^{-1}
a	Bandgap energy quadratic coefficient	1.35
b	Bandgap energy quadratic coefficient	-0.775
c	Bandgap energy quadratic coefficient	0.149
m_e	Effective mass of electron in the CB	4.10×0^{-32} kg
m_{hh}	Effective mass of a heavy hole in the VB	4.19×0^{-31} kg
m_{hl}	Effective mass of a light hole in the VB	5.06×0^{-32} kg

In Fig. 1, it is evident that at low input power, the carrier density has a symmetrical spatial distribution, peaking at the center of the SOA and tailing off towards the input and output facets. This is because the ASE peaks in theses regions as shown in Fig. 2. At high input powers, the carrier density spatial distribution becomes more asymmetrical, with the peak moving towards the input facet. This is caused by the input signal dominating over ASE (Kot and Zdansky, 1992), as shown in Fig. 3.

Bias current effect: The carrier density distribution inside the active region depends on the bias current. Figure 4 represents the influence of the bias current on the free carrier density distribution at -40 dBm input signal and 1537.7 nm signal wavelength. It is clear that the simulated free carrier density in the central of the active region increases with increasing the bias current. This is mainly because the concentration of the injected electrons into the active region increases with the bias current. As a result, the transition region about the junction is far from being depleted of carriers. The transition region contains a large concentration of electrons within the CB and a large concentration of holes within the VB. Consequently, the forward and backward propagating signal photon rates and the total ASE photon rates are increasing with the bias current as shown in Fig. 5 and 6, respectively.

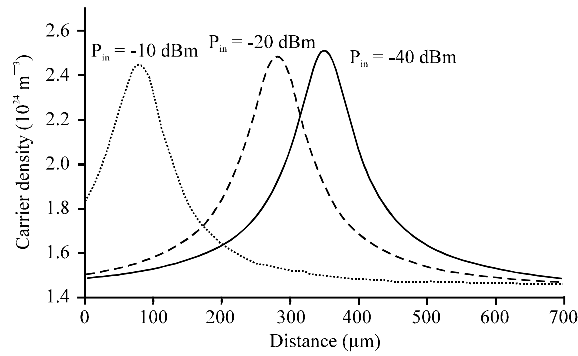

Fig. 1: Carrier density spatial distribution along the active region of the SOA at different input signal powers. The signal wavelength is 1537.7 nm and the bias current is 130 mA

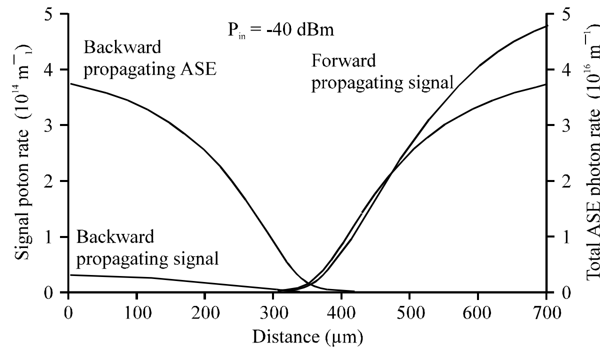

Fig. 2: Forward and backward propagating total ASE and signal photon rates spatial distributions along the active region of the SOA at input signal power = -40 dBm. The signal wavelength is 1537.7 nm and the bias current is 130 mA

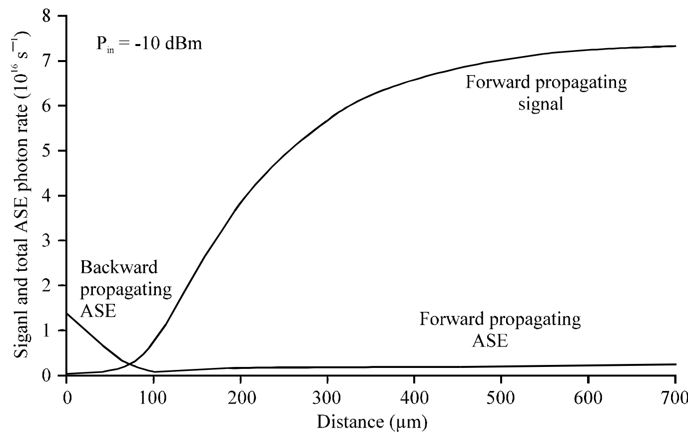

Fig. 3: Forward and backward propagating total ASE and signal photon rates spatial distributions along the active region of the SOA at input signal power = -10 dBm. The signal wavelength is 1537.7 nm and the bias current is 130 mA

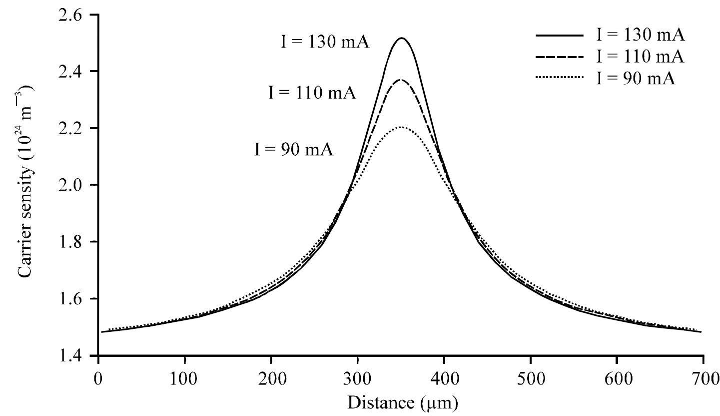

Fig. 4: Carrier density spatial distribution along the active region of the SOA at three different bias currents

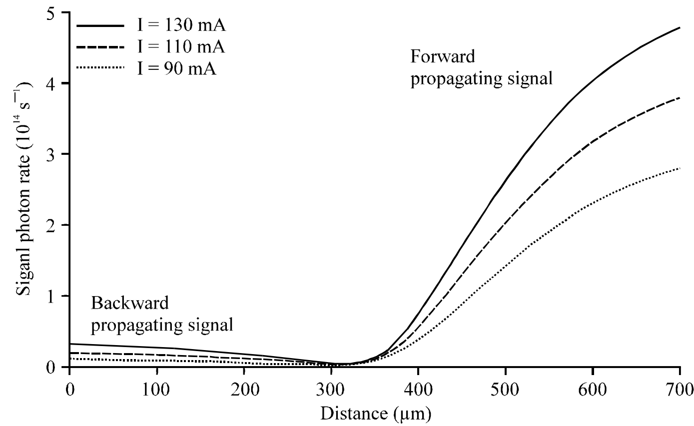

Fig. 5: Forward and backward propagating signal photon rates spatial distributions along the active region of the SOA at three different bias currents

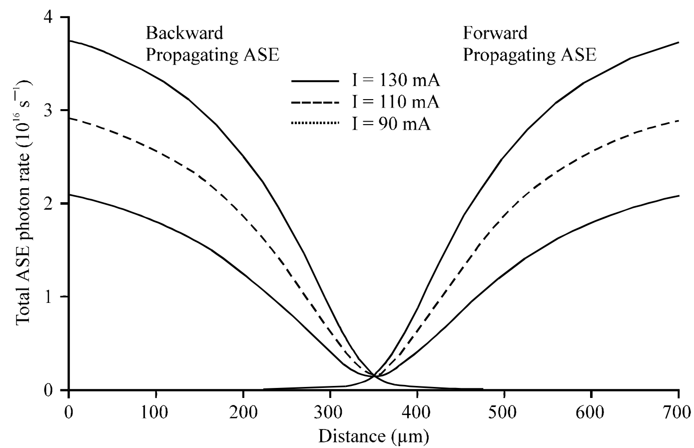

Fig. 6: Forward and backward propagating total ASE photon rates spatial distributions along the active region of the SOA at three different bias currents

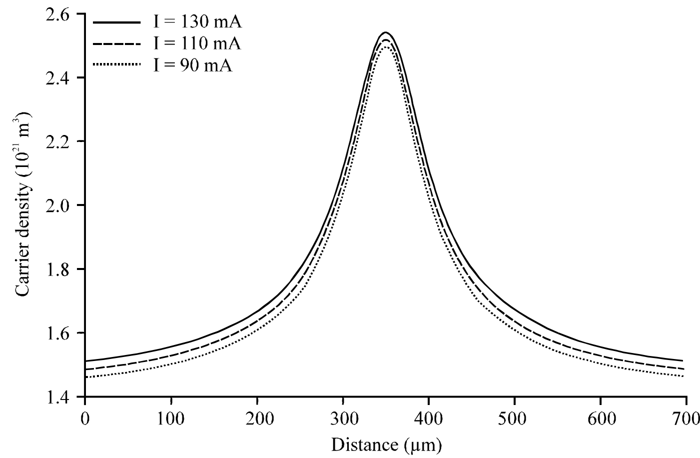

Fig. 7: Carrier density spatial distribution along the active region of the SOA at different values of arsenide molar fraction

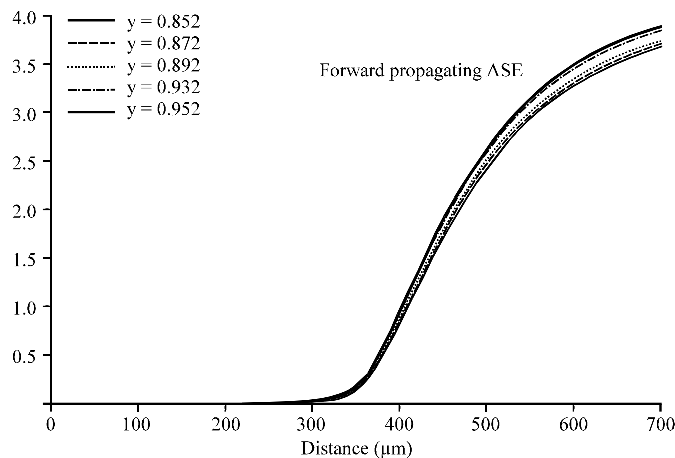

Fig. 8: Forward propagating total ASE photon rates spatial distribution along the active region of the SOA at different values of arsenide molar fraction

Arsenide molar fraction effect: The variation of semiconductor material molar fractions leads to a different compound with new material parameters. Figure 7 shows the simulated free carrier density distribution versus the position along the active region at different values of arsenide molar fraction, y, in InGaAsP active region.

A close inspection of Fig. 7 reveals that the effect of increasing the arsenide molar fraction is slightly decreasing the free carrier density especially at the end facets of the amplifier. The reason of that is when increasing arsenide molar fraction in the InGaAsP active region, the forward and backward ASE photon rates at the end facets of the amplifier, shown in Fig. 8 and 9, respectively, become larger and induce a large consumption of free carriers in the CB.

However, the effect of changing the arsenide molar fraction is significant in the distribution of forward and backward signal photon rates along the active region of the SOA as shown in

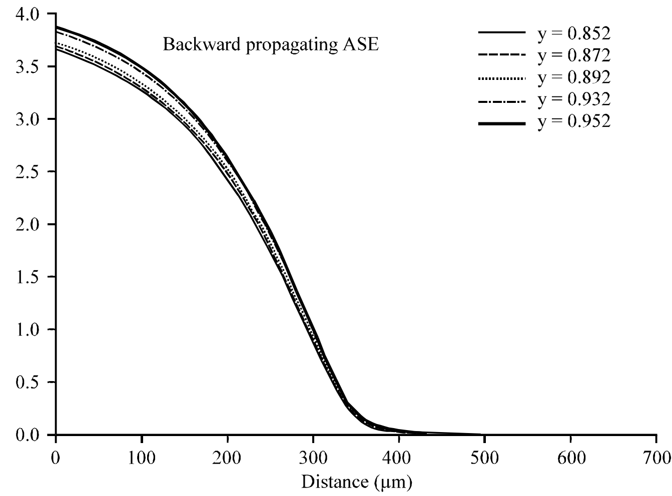

Fig. 9: Backward propagating total ASE photon rates spatial distribution along the active region of the SOA at different values of arsenide molar fraction

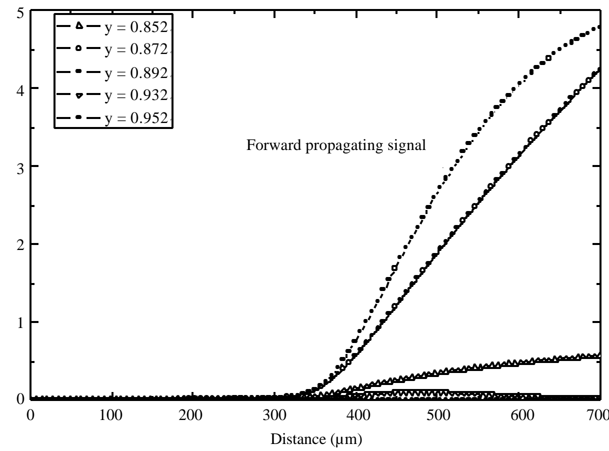

Fig. 10: Forward propagating signal photon rates spatial distribution along the active region of the SOA at different values of arsenide molar fraction

Fig. 10 and 11, respectively. It is well obvious that the forward and backward signal photon rates have a peak value at end facets of the amplifier when the arsenide molar fraction equals 0.892. Any increment or decrement of this value will decrease the peak value of signal photon rates at the end facets. This is due to the best lattice matching between the cladding and active region substrates occurring at y = 0.892.

Temperature effect: Figure 12 depicts the simulated free carrier density distribution versus the position along the active region at different temperatures. It is clear that for a given position in the active region, the simulated free carrier density increases with increasing the temperature. The

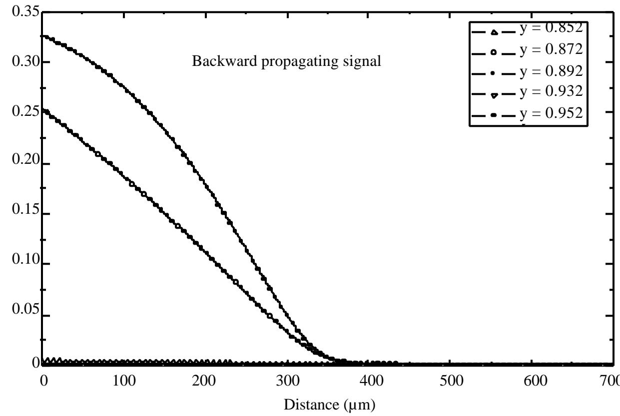

Fig. 11: Backward propagating signal photon rates spatial distribution along the active region of the SOA at different values of arsenide molar fraction

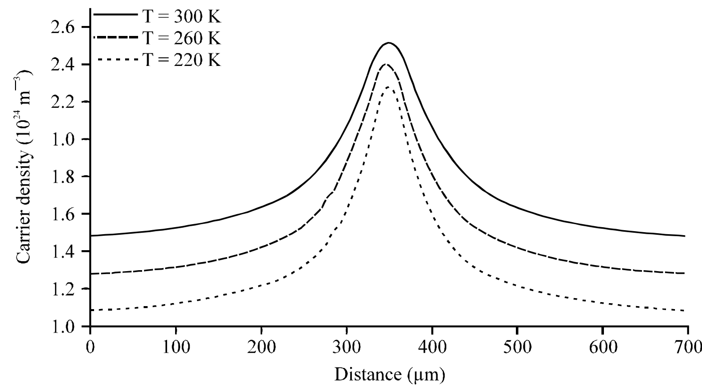

Fig. 12: Carrier density spatial distribution along the active region of the SOA at different temperatures, The signal input power is -40 dBm and the bias current is 130 mA

reason is that as the temperature increases, there is an increased probability of breaking covalent bonds and freeing electrons.

Figure 13 and 14 show the forward and backward propagating signal and total ASE photon rates versus the position along the active region, respectively, at three different temperatures. It can be seen that although the free carrier density increases with increasing the temperature, the forward and backward propagating signal and total ASE photon rates decrease.

This can be explained as follows. As the temperature increases, the free carrier density increases, however, the carrier-carrier scattering at high temperature leads to an increase in the absorption rate (Alfaramawi *et al.*, 2007) and hence the number of carriers available for participating in the processes of stimulated and spontaneous emissions are fewer. In addition, nonradiative recombination increases with increasing temperature for long wavelength materials (Dutta and Wang, 2006) which causes a reduction in the radiative recombination of carriers that affect the amplified signal and ASE. As a result, the forward and backward propagating signal and total ASE photon rates decrease with increasing the temperature.

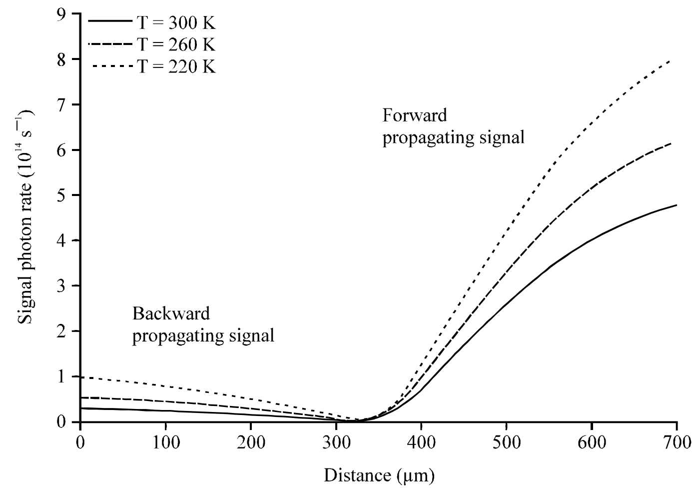

Fig. 13: Forward and backward propagating signal photon rates spatial distribution along the active region of the SOA at different temperatures

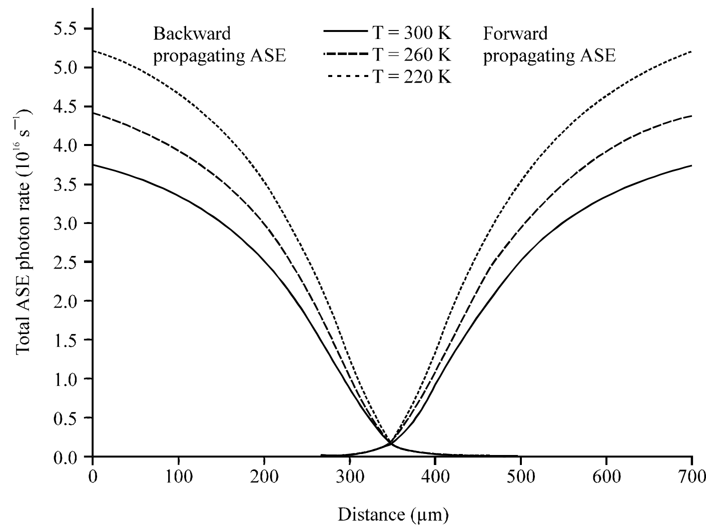

Fig. 14: Forward and backward propagating total ASE photon rates spatial distribution along the active region at different temperatures

CONCLUSION

In this study, the SOA carrier density spatial variation, forward- and backward-propagating signal photon rates and the total ASE photon rates distributions are studied under the effect of the change a set of parameters such as input signal power, bias current, arsenide molar fraction and temperature.

It is found that the average free carrier density decreases with increasing the input power. At low input power, the carrier density has a symmetrical spatial distribution, while at high input powers; the carrier density spatial distribution becomes more asymmetrical. The effect of increasing the bias current is to increase the SOA carrier density and the signal and total ASE photon rates. Although the carrier density increases with increasing the temperature, the signal and total ASE

photon rates decrease with temperature. The forward and backward signal photon rates have a peak value at end facets of the amplifier when the arsenide molar fraction equals 0.892.

REFERENCES

Adachi, S., 1992. Physical Properties of III-V Semiconductor Compounds: InP, InAs, GaAs, GaP, InGaAs and InGaAsP. Wiley-VCH, New York, USA., ISBN-13: 9780471573296, Pages: 318.

Agrawal, G.P., 2002. Fiber-Optic Communication Systems, Volume 1. 3rd Edn., Wiley-Interscience, New York, USA., ISBN-13: 9780471215714, Pages: 546.

Alfaramawi, K., O. Mahran, W. El-Shirbeeny and S. Abboudy, 2007. Steady-state properties of the wideband semiconductor optical amplifier. Optoelectron. Adv. Mater. Rapid Commun., 1: 571-575.

Connelly, M.J., 2001. Wideband semiconductor optical amplifier steady-state numerical model. IEEE J. Quantum Electron., 37: 439-447.

Dutta, N.K. and Q. Wang, 2006. Semiconductor Optical Amplifiers. World Scientific, Singapore, ISBN: 9789812563972 Pages: 297.

Gillner, L., 1992. Comparative study of some travelling-wave semiconductor laser amplifier models. IEEE Proc. J. Optoelectron., 139: 339-347.

Kot, M. and K. Zdansky, 1992. Measurement of radiative and nonradiative recombination rate in InGaAsP-InP LED's. IEEE J. Quantum Electron., 28: 1746-1750.

Lowery, A.J., 1990. Amplified spontaneous emission in semiconductor laser amplifiers: Validity of the transmission-line laser model. IEEE Proc. J. Optoelectron., 137: 241-247.

Marcuse, D., 1983. Computer model of an injection laser amplifier. IEEE J. Quantum Electron., 19: 63-73.

Nilsson, N.G., 1978. Empirical approximations for the Fermi energy of a semiconductor with parabolic bands. Applied Phys. Lett., 33: 653-654.

Olshansky, R., C.A. Su, J. Manning and W. Powazinik, 1984. Measurement of radiative and nonradiative recombination rates in InGaAsP and AlGaAs light sources. IEEE J. Quantum Electron., 20: 838-854.

Wolff, P.A., 1962. Theory of the band structure of very degenerate semiconductors. Phys. Rev., 126: 405-412.